JOURNAL OF AIRCRAFT
Vol. 44, No. 3, May–June 2007

Two-Dimensional Unsteady Aerodynamic Application to Higher Harmonic Control Test Data

Mark. A. Couch*
University of Illinois, Champaign, Illinois 61820
and
E. Roberts Wood†
Naval Postgraduate School, Monterey, California 93943

DOI: 10.2514/1.23369

In 1982, flight tests were conducted on a modified OH-6A helicopter that incorporated an active higher harmonic control system to reduce vibratory loads on the rotor system. While reducing vibrations up to 90%, open-loop higher harmonic control data showed significant reductions in the main rotor shaft torque and engine power indicating that higher harmonic control may be also providing performance improvements. In this study, unsteady, rotary-wing, potential flow theory for a thin, oscillating airfoil is used to explain the mechanism behind the performance improvements seen on the OH-6A. Equations for the 2-D, unsteady, rotary-wing aerodynamic forces and moments with a finite number of wakes, or shed layers of vorticity, beneath the rotor are developed and applied specifically to the pitch and flap oscillations seen in the hover flight-test data. A modified finite-wake lift deficiency function is developed for this finite-wake theory that is analogous to the classical Theodorsen and Loewy lift deficiency functions, and is used in used to calculate the horizontal time-averaged propulsive force (negative drag) derived by Garrick to show that unsteady aerodynamics can provide the order of magnitude effects necessary to quantify the performance improvements seen on the OH-6A.

Nomenclature

a	=	nondimensional elastic axis location measured from midchord
b	=	semichord length
$C(k)$	=	Theodorsen's lift deficiency function
$C(k, \hat{h}, m)$	=	Loewy's lift deficiency function
$C_N(k, \hat{h}, m)$	=	finite-wake lift deficiency function
F	=	real part of lift deficiency function
G	=	imaginary part of lift deficiency function
$H_n^{(2)}$	=	Hankel function (complex Bessel function) of second kind of order n, $J_n - Y_n$
h	=	vertical displacement (plunge) of airfoil above the flapping plane
$\hat{h}$	=	nondimensional distance between layers of shed vorticity (wake spacing), $2\pi v/bQ\Omega$
h_0	=	amplitude of deflection in simple harmonic motion
J_n	=	real part of complex Bessel function of order n
k	=	reduced frequency, $\omega b/v$ (fixed wing), or $\omega b/\Omega r$ (rotary wing)
M_α	=	aerodynamic moment about the elastic axis (positive clockwise)
m	=	ratio of oscillation frequency to rotational frequency, ω/Ω
N	=	number of wakes for a single-blade rotor
n	=	revolution number
P	=	aerodynamic force on the airfoil
Q	=	total number of blades
q	=	blade number
r	=	blade section radius from center of rotation
t	=	time
V	=	forward airspeed
v	=	freestream velocity
W	=	Loewy's wake weighting function
W_N	=	finite-wake weighting function
w	=	downwash velocity
x	=	nondimensional distance from midchord
Y_N	=	imaginary part of complex Bessel function
α	=	rotational displacement (pitch) about elastic axis of airfoil from reference angle
α_0	=	amplitude of rotation in simple harmonic motion
Γ	=	total circulation around the airfoil
γ_a	=	vorticity generated by reference airfoil
γ_{nq}	=	vorticity generated by qth blade in nth revolution
μ	=	advance ratio, $V/\Omega r$
ξ	=	nondimensional distance from midchord
ρ	=	density of air
Φ	=	velocity potential
φ_1	=	phase angle between initiation of rotation input and arbitrary reference point
φ_2	=	phase angle between initiation of amplitude input and arbitrary reference point
ψ_q	=	phase angle by which motion of qth blade leads reference blade
Ω	=	rotational frequency of rotor
ω	=	frequency of oscillation

Presented as Paper 6017 at the 2002 Biennial International Powered Lift Conference and Exhibit, Williamsburg, VA, 5–7 November 2002; received 21 February 2006; revision received 26 July 2006; accepted for publication 31 January 2007.

*Executive Officer and Associate Professor of Naval Science, 505 East Armory Avenue, MC-536. Senior Member AIAA.

†Professor Emeritus, Department of Mechanical and Astronautical Engineering, MAE/Wd, 700 Dyer Road. Associate Fellow AIAA.

I. Introduction

IN 1982, flight tests were conducted on a modified Hughes OH-6A helicopter that incorporated an active higher harmonic control (HHC) system [1]. HHC is an active control concept that introduces control inputs into the nonrotating reference frame at the rotor hub to reduce the vibratory loads caused by the aerodynamic loads in the rotating reference frame of the hub. In contrast, conventional passive control concepts, such as vibration absorbers, vibration isolators, and bifilar absorbers, attempt to reduce vibrations after all the

aerodynamic and mechanical loads have transferred from the rotating reference frame to the nonrotating reference frame, and further to the airframe itself. The flight-test results showed vibration reductions up to 90% could be achieved. Additionally, the open-loop data showed significant reductions in the main rotor shaft torque and engine power indicating that HHC may be providing performance improvements along with the vibration reduction. Because HHC was designed to reduce the aerodynamic loads before they are transmitted to the airframe, a correlation between reduced vibrations and improved aerodynamics was postulated that could lead to performance benefits seen in the OH-6A flight tests.

Cheng et al. [2] developed a theoretical basis for HHC performance improvements for 2/rev (or 2P) inputs using a blade similar to the H-60 by showing that a reduction in profile drag could reduce rotor power up to 16% when properly phased. This paper, however, will develop an alternate theoretical basis for improved HHC performance for 4P inputs on actual OH-6A flight-test data showing that the rotary-wing version of the thin oscillating airfoil theory can produce a propulsive force of sufficient magnitude that reduces the induced drag on the airfoil. This reduction in induced drag is due to the coupled pitch–plunge motion associated with the inherent rotor blade flapping motion combined with the small-angle pitch motion introduced by the OH-6A HHC controller at certain phase relationships to the flapping rotor blade. Additionally, a review of a few other HHC flight-test and wind tunnel test programs will be made to ascertain why a performance improvement may or may not have been seen on the Boeing CH-47D Chinook scaled rotor [3], Aérospatiale SA-349 Gazelle [4], and Sikorsky S-76A [5,6].

II. OH-6A HHC Flight-Test Program

The modified OH-6A used for the HHC flight-test program had the factory-installed primary actuators replaced with 3000 psi hydraulically boosted, high-frequency actuators capable of inputs up to 90 Hz as shown in Fig. 1. The actuators had a collective blade angle authority of 2 deg, approximately 11% of total collective pitch range. Higher harmonic blade pitch control was achieved by superimposing 4P (32 Hz) nonrotating swashplate input motion upon pilot cyclic and collective control inputs. The 4P inputs in the nonrotating reference frame generated 3P and 5P inputs in the rotating reference frame, which corresponds to the frequencies at which the primary vibrational loads are transmitted to the fuselage.

After the 3000 psi actuators were installed, initial ground tests indicated that the system was incapable of transmitting the desired 32-Hz inputs into main rotor blade pitch motion. It was determined that freeplay, typical of the unboosted control system, was the source of this lost motion. Considerable effort was then taken to eliminate excessive freeplay from the system by use of precision tolerance roller bearings, bolts, bushings, metal-to-metal rod end bearings, and a redesigned, less-flexible mixing unit manufactured with ANSI

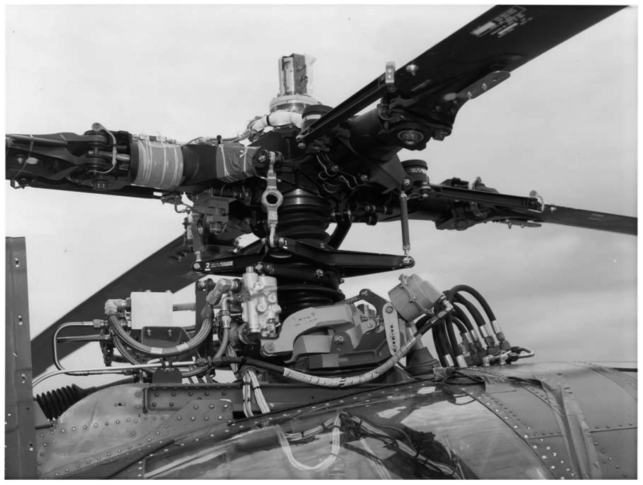

Fig. 1 Right lateral actuator installed between mixing unit and swashplate.

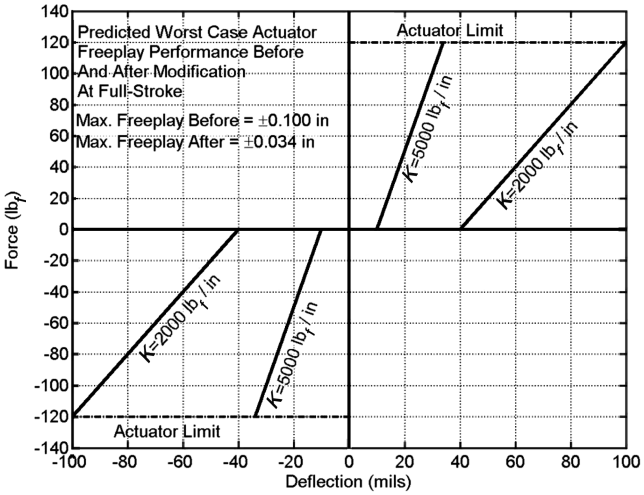

Fig. 2 Comparison of freeplay on OH-6A before ($K = 2000$ lb$_f$/in.) and after ($K = 5000$ lb$_f$/in.) actuator modification.

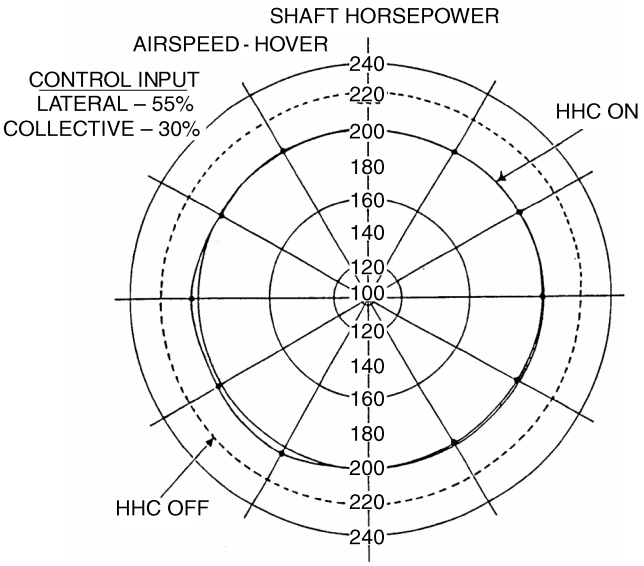

Fig. 3 Effect of HHC on main rotor power in hover.

4130 steel. Figure 2 shows the result of this six-month effort to minimize freeplay, resulting in a two-thirds reduction in the amount of freeplay and an increase in system stiffness by a factor of 2.5. This modified, reduced freeplay system was capable of transmitting an equivalent ± 0.5 deg input from the actuator into ± 0.33 deg blade pitch motion. Although freeplay was not completely eliminated, its reduction ensured that actuator inputs would be more directly applied to the vibrations caused by the aerodynamic loads, and hence to the aerodynamic forces and moments themselves.

In addition to reducing the vibration levels on the aircraft, the HHC system showed a reduction in the main rotor torque at airspeeds below 100 knots. Figures 3–6 plot the main rotor shaft horsepower at various phase input relationships for lateral swashplate excitation equivalent to ± 0.33 deg of blade motion for hover flight and forward airspeeds of 60, 80, and 100 knots, respectively. Additional plots showing corresponding reductions in engine power are contained in [7] that independently verify this performance benefit and indicate that reductions in main rotor power were not being made at the expense of engine power. For each run, a baseline power level was established with HHC "off," and then with HHC "on"; data were recorded in 30 deg increments of controller phase setting. (It should be noted that due to the limited scope of the performance tests on the OH-6A, the controller phase setting cannot be directly correlated with the frequency ratio m, discussed in the next section on Thin

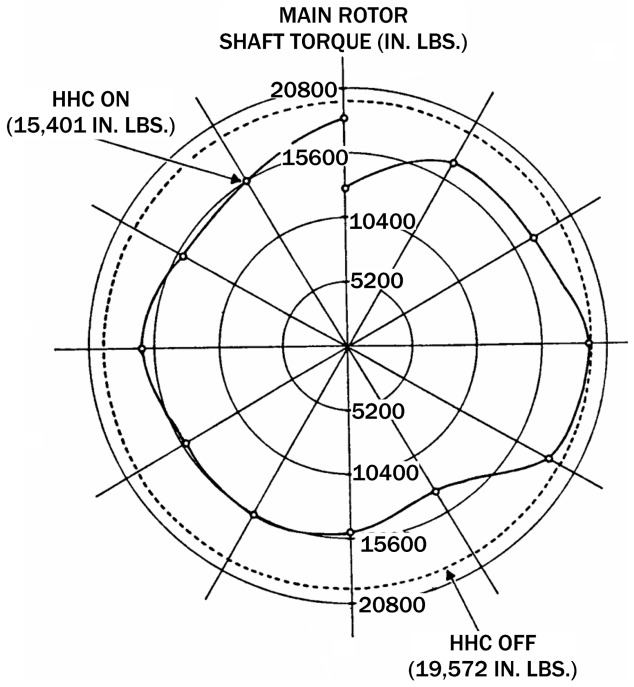

Fig. 4 Effect of HHC on main rotor power at 60 knots.

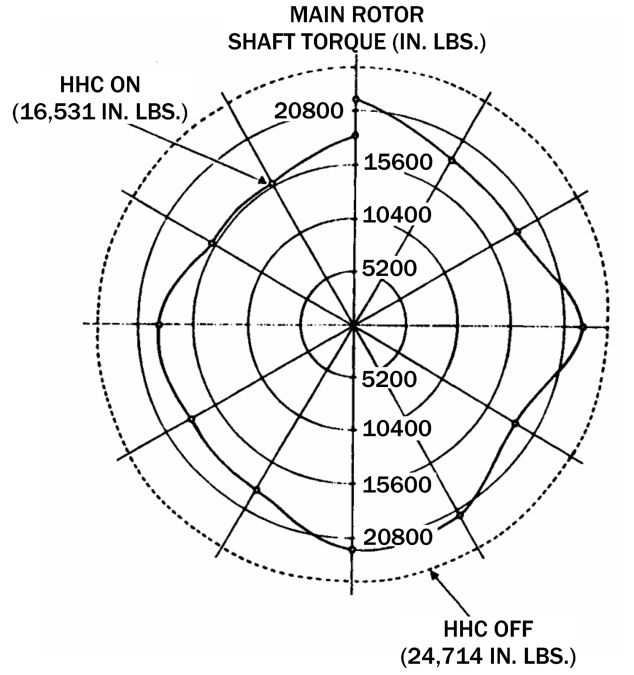

Fig. 5 Effect of HHC on main rotor power at 80 knots.

Oscillating Airfoil Theory.) From Figs. 3–6, the following conclusions can be drawn:

1) The power savings disappear at 100 knots.

2) The hover, 60, and 80 knots cases indicate a power saving of 10–15%.

3) Certain phase settings appear to provide a greater power savings than others.

4) Closure at the 0 deg phase relationship was poor after a 20-min test sequence.

III. Thin Oscillating Airfoil Theory

The aerodynamic forces and moments on an oscillating airfoil for the fixed-wing case as determined by Theodorsen [8] are based on

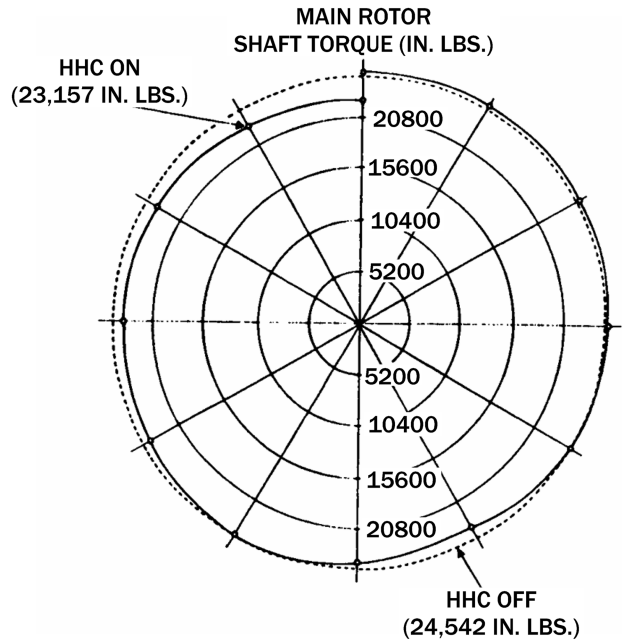

Fig. 6 Effect of HHC on main rotor power at 100 knots.

potential flow theory and application of the Kutta condition. Potential flow theory reduces to Laplace's equation for the case of incompressible subsonic flow:

$$\frac{\partial^2 \Phi}{\partial x^2} + \frac{\partial^2 \Phi}{\partial y^2} = 0 \tag{1}$$

Because potential flow theory follows the principle of superposition, the potentials can be treated as two types: noncirculatory and circulatory. The noncirculatory terms result primarily from the effects of the freestream airflow with the airfoil. The circulatory terms result from the vorticity generated in the wake of the airfoil.

The aerodynamic forces and moments on a thin airfoil are depicted in Fig. 7. Integrating the pressure difference across the airfoil determined from the generalized Bernoulli equation, Theodorsen wrote the forces and moments as

$$P = -\pi\rho b^2(v\dot{\alpha} + \ddot{h} - ba\ddot{\alpha}) - 2\pi\rho v b C(k)\left[v\alpha + \dot{h} + b\left(\frac{1}{2} - a\right)\dot{\alpha}\right] \tag{2}$$

and

$$M_\alpha = -\pi\rho b^2\left[\left(\frac{1}{2} - a\right)vb\dot{\alpha} + b^2\left(\frac{1}{8} + a^2\right)\ddot{\alpha} - ab\ddot{h}\right] + 2\pi\rho v b^2\left(a + \frac{1}{2}\right)C(k)\left[v\alpha + \dot{h} + b\left(\frac{1}{2} - a\right)\dot{\alpha}\right] \tag{3}$$

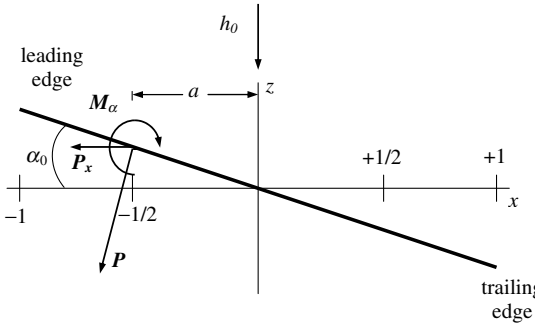

Fig. 7 Parameters of a thin airfoil nondimensionalized by the semichord *b*.

where $C(k)$ is Theodorsen's well-known lift deficiency function, which is defined as

$$C(k) = \frac{H_1^{(2)}}{H_1^{(2)} + iH_0^{(2)}} \tag{4}$$

The lift deficiency function can be separated into its real and imaginary parts as

$$C(k) = F(k) + iG(k) \tag{5}$$

where

$$F(k) = \frac{J_1(J_1 + Y_0) + Y_1(Y_1 - J_0)}{(J_1 + Y_0)^2 + (Y_1 - J_0)^2} \tag{6}$$

and

$$G(k) = -\frac{Y_1 Y_0 + J_1 J_0}{(J_1 + Y_0)^2 + (Y_1 - J_0)^2} \tag{7}$$

with all Bessel functions evaluated at the reduced frequency k. A typical plot of $F(k)$ and $G(k)$ is shown in Fig. 8. Because the behavior of the functions $F(k)$ and $G(k)$ as k approaches zero and infinity is not easily seen, a semilogarithmic plot of Theodorsen's lift deficiency function [9] is shown in Fig. 9. This semilog plot looks

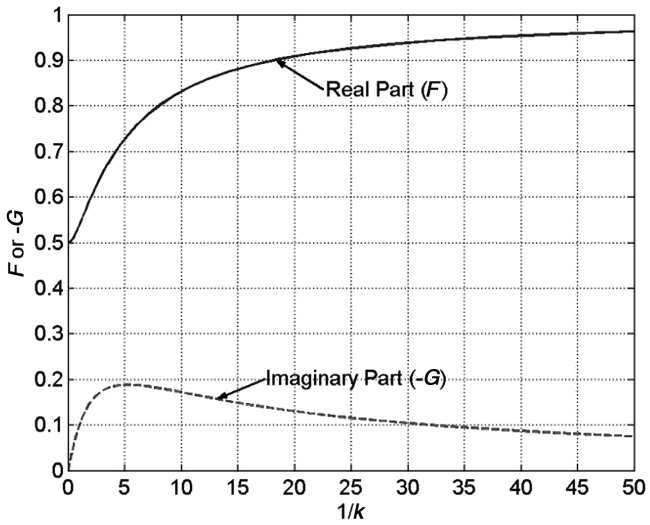

Fig. 8 Conventional plot of Theodorsen's lift deficiency function.

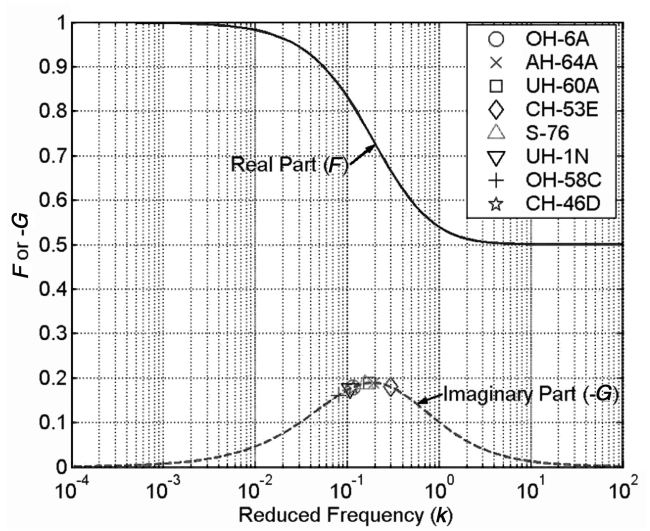

Fig. 9 Semilogarithmic plot of Theodorsen's lift deficiency function with n/rev reduced frequencies.

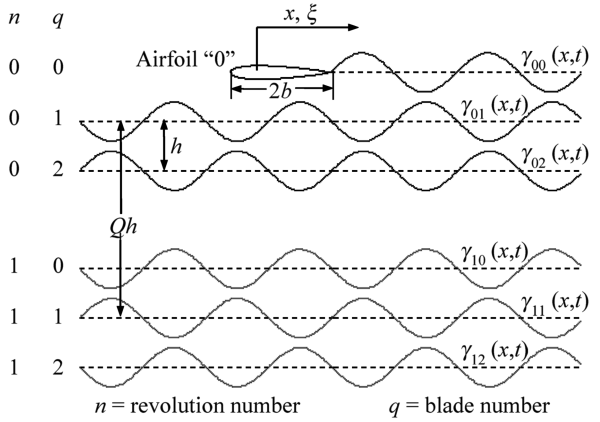

Fig. 10 Aerodynamic model for a multiblade rotor system.

similar to a Bode plot of the complex lift deficiency function, $C(k)$, where $F(k)$ is the predominant magnitude term and $G(k)$ is the term that influences the phase angle. Superimposed on the plots in Fig. 9 are the values for $G(k)$ for selected helicopters at their n/rev-reduced frequencies. It should be noted that for the helicopters studied, all have their n/rev reduced frequencies in a range where $G(k)$ is noticeably nonzero, thus producing a natural phase relationship in the lift of a rotor blade.

Loewy showed that the aerodynamic forces and moments on an oscillating airfoil for the rotary-wing case are more complex than the fixed-wing counterpart [10]. He determined these forces and moments for the hover case, where $k = \omega b/\Omega R$, but used a slightly different approach to the problem by solving the integral downwash equation that led to an equation for the pressure distribution, which is in the same form as Theodorsen. Loewy then defined a modified lift deficiency function, and stated that the integration of the pressure distribution across the airfoil would be identical to Theodorsen, making the expression for forces and moments the same, except for a modified lift deficiency function.

Because of the periodic nature of a rotating blade, Loewy first set up an accounting system for the wakes generated by the previous blades in the same revolution and all blades in the previous revolutions as shown in Fig. 10. He used two indices to account for the vorticity shed by a given wake: n indicated the revolution and q indicated the blade whose wake it was. The induced velocity or downwash resulting from an element of vorticity was obtained from the Biot–Savart Theorem,

$$\mathrm{d}\, w(x) = \frac{1}{2\pi}\left(\frac{\gamma_{nq}(x-\xi)\,\mathrm{d}\xi}{(x-\xi)^2 + (nQ+q)^2\hat{h}^2}\right) \tag{8}$$

Writing the integrals involving the bound vorticity and the vorticity in the wake of the reference airfoil separately from the rows of vorticity below the plane of the rotor yields

$$\begin{aligned} w(x) = -\frac{1}{2\pi}\Bigg[&\int_{-1}^{1}\frac{\gamma_a(\xi)\,\mathrm{d}\xi}{x-\xi} + \int_{1}^{\infty}\frac{\gamma_{00}(\xi)\,\mathrm{d}\xi}{x-\xi} \\ &+ \sum_{q=1}^{Q-1}\sum_{n=0}^{\infty}\int_{-\infty}^{\infty}\frac{\gamma_{nq}(\xi)(x-\xi)\,\mathrm{d}\xi}{(x-\xi)^2 + (nQ+q)^2\hat{h}^2} \\ &+ \sum_{n=1}^{\infty}\int_{-\infty}^{\infty}\frac{\gamma_{n0}(\xi)(x-\xi)\,\mathrm{d}\xi}{(x-\xi)^2 + n^2Q^2\hat{h}^2}\Bigg] \end{aligned} \tag{9}$$

The first integral represents the effects of the freestream on the airfoil (noncirculatory terms). The second integral represents the velocity created by the vorticity generated by the reference wake (circulatory term). The third and fourth integrals represent the velocity created by the vorticity generated by previous blades or in previous revolutions (circulatory terms). The primary differences between Loewy's and Theodorsen's theories are the terms that account for the vorticity generated by previous blades or in previous revolutions.

Loewy shows that the vorticity shed by the qth blade in the nth revolution is

$$\gamma_{nq} = ik\Gamma e^{i(\psi_q - k\xi - 2\pi mq/Q - 2\pi mn)} \tag{10}$$

The frequency ratio m is directly related to the phase angle relationship between the input frequency of oscillation and a reference point on the rotor. This phase angle relationship determines how the flow over the airfoil interacts with the shed layers of vorticity, and how each layer of vorticity interacts with the other layers. Because of the periodicity of ψ_q in a hover, the multiblade case can be reduced to a case with a single rotor blade for comparison with Theodorsen.

Substituting the vorticity expression from Eq. (10) into the integral downwash Eq. (9) and applying the Kutta condition, Loewy developed the generalized Bernoulli equation in the same form as Theodorsen, but with a modified lift deficiency function as follows:

$$C'(k, \hat{h}, m) = \frac{H_1^{(2)} + 2J_1 W(k, \hat{h}, m)}{H_1^{(2)} + iH_0^{(2)} + 2(J_1 + iJ_0)W(k, \hat{h}, m)} \tag{11}$$

where $W(k, h, m)$ is the wake weighting function defined by

$$W(k, \hat{h}, m) = \frac{1 + \sum_{q=1}^{Q-1} (e^{k\hat{h}Q} e^{i2\pi m})^{(Q-q)/Q} e^{i\psi_q}}{e^{k\hat{h}Q} e^{i2\pi m} - 1} \tag{12}$$

It can be shown that as $W(k, \hat{h}, m)$ approaches zero, $C'(k, \hat{h}, m) = C(k)$, which corresponds to infinite wake spacing ($\hat{h} \to \infty$).

Loewy's theory for an infinite number of wakes can be reduced to the case of a finite number of wakes by modifying the wake weighting function [9] while maintaining the same definition of the lift deficiency function. Because the lift deficiency function is still in the same form as Theodorsen, the equations for the aerodynamic forces and moments will be the same, but with a modified finite-wake lift deficiency function. Rederiving Loewy's integral downwash equation to a finite number N of revolutions yields

$$w(x) = -\frac{1}{2\pi}\left[\int_{-1}^{1} \frac{\gamma_a(\xi)\,d\xi}{(x-\xi)} - ik\Gamma \int_{1}^{\infty} \frac{e^{-ik\xi}\,d\xi}{(x-\xi)} + \pi k\Gamma e^{-ikx}\left(\sum_{q=1}^{Q-1} e^{-i(2\pi q/Q - \psi_q)} \sum_{n=0}^{N} e^{-i2\pi mn} e^{-k(nQ+q)\hat{h}} + \sum_{n=1}^{N} e^{-i2\pi mn} e^{-nQk\hat{h}}\right)\right] \tag{13}$$

The terms enclosed by the parentheses can be defined as the finite-wake weighting function, or

$$W_N(k, \hat{h}, m) = \sum_{q=1}^{Q-1} e^{-i(2\pi q/Q - \psi_q)} \sum_{n=0}^{N} e^{-i2\pi mn} e^{-k(nQ+q)\hat{h}} + \sum_{n=1}^{N} e^{-i2\pi mn} e^{-nQk\hat{h}} \tag{14}$$

It can be shown that for a hover this modified wake weighting function is periodic once the relationship ψ_q is known, and the multiblade rotor can be reduced to a single-blade rotor with modified wake spacing and frequency ratio. For the case of the single-blade rotor ($Q = 1$),

$$W_N(k, \hat{h}, m) = \sum_{n=1}^{N} e^{-i2\pi mn} e^{-nk\hat{h}} \tag{15}$$

It should be noted that the finite-wake weighting function does not have the singularity noted in the Loewy wake weighting function in [10].

The solution to the remainder of the finite-wake problem is identical to Loewy, but using the modified finite-wake lift deficiency function. To distinguish the finite-wake lift deficiency function from Loewy's lift deficiency function, the former is denoted with the subscript N as follows:

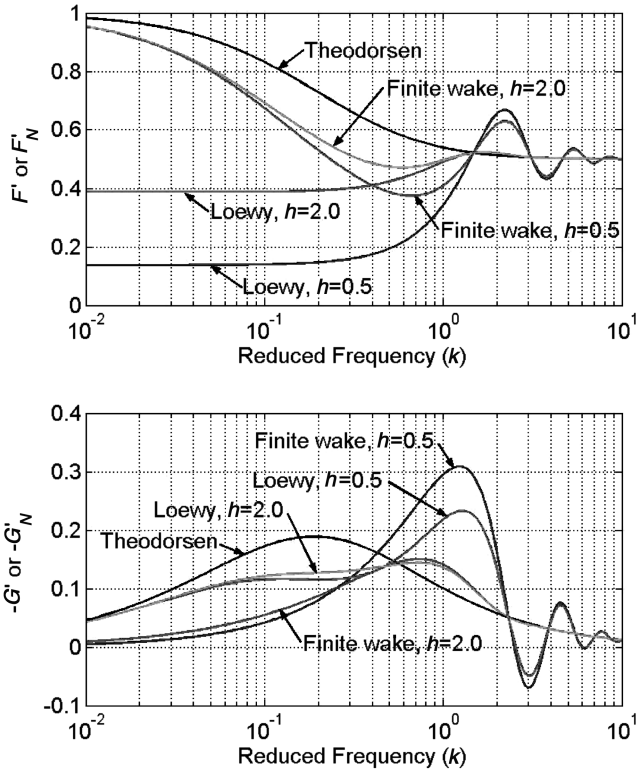

Fig. 11 Lift deficiency functions for $m = 0$.

$$C'_N(k, \hat{h}, m) = \frac{H_1^{(2)} + 2J_1 W_N(k, \hat{h}, m)}{H_1^{(2)} + iH_0^{(2)} + 2(J_1 + iJ_0)W_N(k, \hat{h}, m)} \tag{16}$$

For the case of a single wake, the wake weighting function reduces to

$$W_1 = e^{-(i2\pi m + k\hat{h})} \tag{17}$$

Comparisons of the real and imaginary parts of the Loewy lift deficiency function to the single-wake lift deficiency function are shown in Figs. 11 and 12 for different combinations of wake spacing and frequency ratio (wake phasing).

The case where $m = 0$ (Fig. 11) corresponds to the wakes being in phase with the oscillatory frequency. The Loewy lift deficiency function exhibits a singularity in the solution as $k \to 0$, which is evident in the plots of the real and imaginary parts of the lift deficiency function, making the theory inaccurate at very low reduced frequencies. The single-wake model exhibits behavior similar to Theodorsen, but with some oscillatory behavior.

The case where $m = 0.5$ (Fig. 12) corresponds to wake phasing of 180 deg (out of phase). The Loewy model is comparable to Theodorsen at most wake spacings. However, the real part of the single-wake lift deficiency function is greater than one for certain ranges of reduced frequencies. This enhancement in the real part of the single-wake lift deficiency function causes the magnitude of $C(k)$ to be greater than 1.0, and thus the "lift deficiency" function becomes a "lift efficiency" function. Also, it can be seen that the absolute value of the imaginary part also increases in the same ranges, which further increase the effect the lift deficiency function has on the aerodynamic forces and moments. Figure 13 is a schematic showing how optimally phased wakes could enhance the lift deficiency function.

IV. Unsteady Aerodynamic Application to HHC Performance

A. Propulsive Force (Negative Drag)

In two series of experiments, Katzmayr [11] conducted one of the earliest investigations of the effect that an oscillating airfoil had on

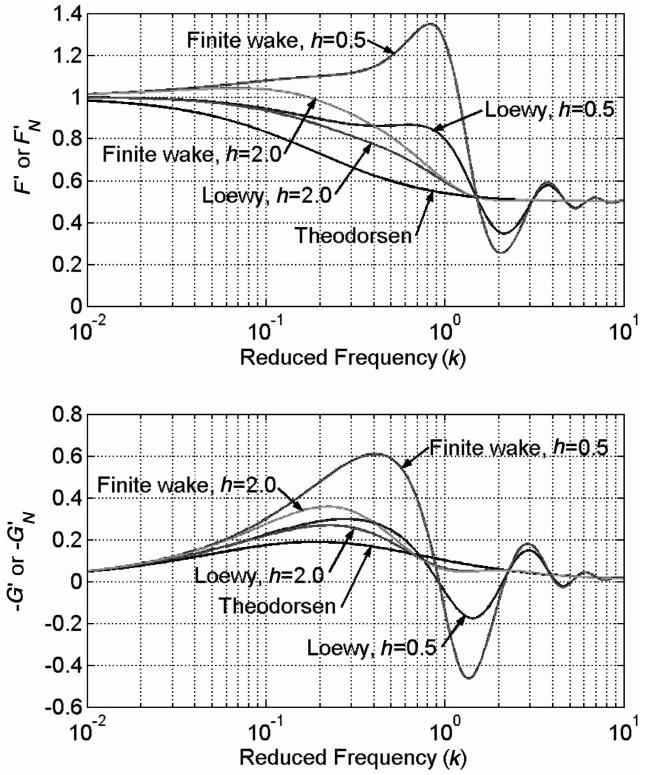

Fig. 12 Lift deficiency functions for $m = 0.5$.

resultant drag. He measured a negative drag, or propulsive force, for certain combinations of velocity and frequency of oscillation. This discovery, later known as the "Katzmayr effect," helped answer the question of how birds propelled themselves through the air. Garrick [12] applied the equations of motion developed by Theodorsen to obtain a closed-form solution to the "Katzmayr effect." Garrick determined the time-averaged horizontal force to be

$$\bar{P}_x = \pi\rho b\omega^2\left(h_o^2(F^2+G^2) + b^2\alpha_o^2\left\{(F^2+G^2)\left[\frac{1}{k^2}+\left(\frac{1}{2}-a\right)^2\right]\right.\right.$$
$$+\frac{1}{2}\left(\frac{1}{2}-a\right) - F\left(\frac{1}{2}-a+\frac{1}{k^2}\right) - \frac{G}{k}\left(a+\frac{1}{2}\right)\Big\}$$
$$+ b\alpha_o h_o\left\{\left(-\frac{1}{k}(F^2+G^2)+\frac{F}{2k}+\frac{G}{2}\right)\sin(\varphi_2-\varphi_0)\right.$$
$$\left.\left.+\left[\left(\frac{1}{2}-a\right)(F^2+G^2)+\frac{1}{2}\left(\frac{1}{2}+\frac{G}{k}-F\right)\right]\cos(\varphi_2-\varphi_1)\right\}\right) \tag{18}$$

Because propulsive force is analogous to negative drag, it is convenient to define a propulsive force coefficient as $C_{Px} = \bar{P}_x/\rho v^2 b$, and if it is assumed that the pitch and plunge input oscillations are in phase with each other, the propulsive force coefficient for coupled pitch–plunge becomes

$$C_{Px} = \pi k^2\left(\frac{h_0^2}{b^2}(F^2+G^2) + \alpha_0^2\left\{(F^2+G^2)\left[\frac{1}{k^2}+\left(\frac{1}{2}-a\right)^2\right]\right.\right.$$
$$+\frac{1}{2}\left(\frac{1}{2}-a\right) - F\left(\frac{1}{2}-a+\frac{1}{k^2}\right) - \left(\frac{1}{2}+a\right)\frac{G}{K}\Big\}$$
$$\left.+\alpha_0\frac{h_0}{b}\left[\left(\frac{1}{2}-a\right)(F^2+G^2)+\frac{1}{2}\left(\frac{1}{2}-\frac{G}{k}-F\right)\right]\right) \tag{19}$$

Because the Loewy and finite-wake lift deficiency functions were developed in a manner similar to Theodorsen, the real and imaginary parts of either function could be substituted into Garrick's propulsive

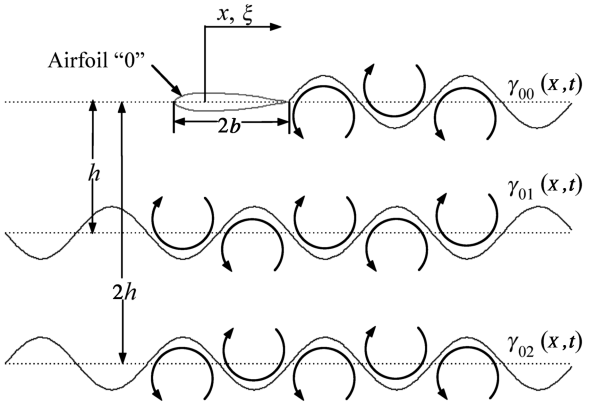

Fig. 13 Optimally phased wakes for $m = 0.5$.

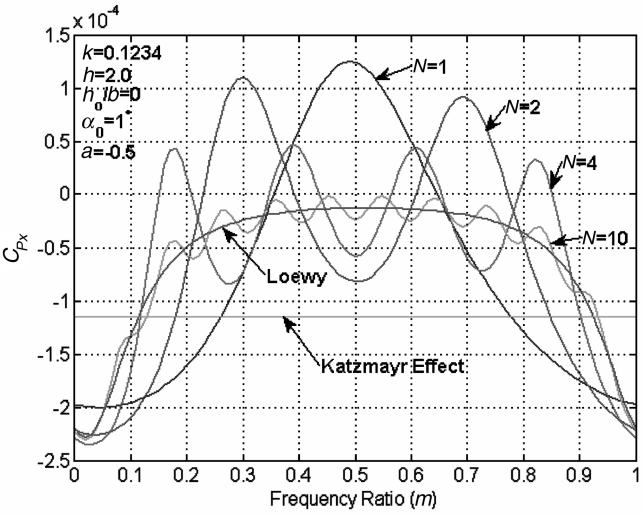

Fig. 14 Propulsive force coefficient for pitch only.

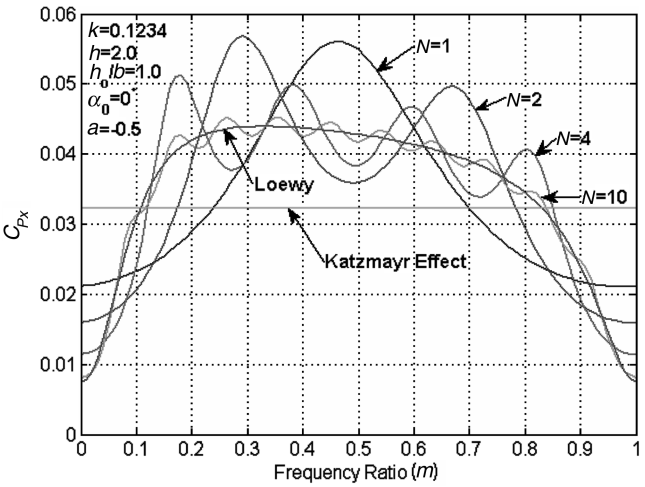

Fig. 15 Propulsive force coefficient for plunge only.

force equation. Plots of the propulsive force coefficient as a function of frequency ratio (i.e., phase relationship) are shown for pitch only (Fig. 14), plunge only (Fig. 15), and coupled pitch–plunge (Fig. 16) oscillations for a single wake of shed vorticity beneath the rotor blade. An important point to be drawn from Figs. 14–16 is that the propulsive force coefficient using coupled pitch–plunge is more than just the summation of the propulsive force provided individually by pure plunge and pure pitch. The cross-coupling terms in Eq. (19) are a

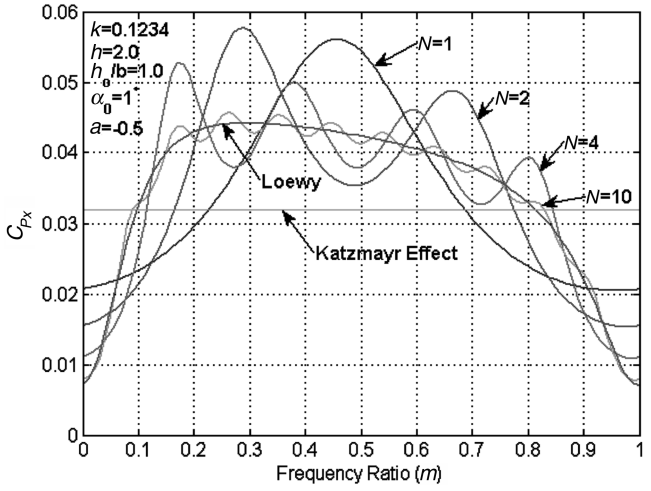

Fig. 16 Propulsive force coefficient for coupled pitch–plunge.

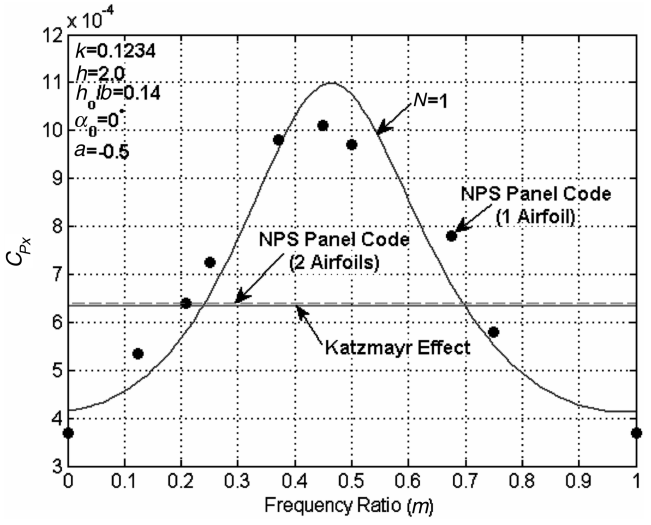

Fig. 17 Comparison of single-wake propulsive force coefficient in plunge only to NPS panel code of [13].

result of the added potentials created by an airfoil oscillating in both pitch and plunge.

To gain confidence that the propulsive force coefficients shown in Figs. 14–16 are reasonable, an unsteady panel code developed at the Naval Postgraduate School [13] for an inviscid, incompressible fluid was modified to include the effects of a single wake beneath the reference airfoil. A comparison of the propulsive force coefficient determined by the single-wake theory and the panel code for plunge only is shown in Fig. 17. It can be seen that both methods agree very well with each other, giving confidence in the application of the single-wake theory.

B. OH-6A HHC Performance Benefit

Because the thin, oscillating airfoil theory for rotary wing developed in this paper is for the hover case, the performance benefits seen in hover for the OH-6A (Fig. 3) will be examined to determine if unsteady aerodynamics can provide the order of magnitude effects necessary to account for the reduction in main rotor power. The change in shaft horsepower from HHC off to HHC on in a hover is approximately 20 hp, which converts to 217.5 ft · lb of torque. The change of torque is a direct measure of the reduction in induced drag on the rotor blades because the same amount of lift must still be generated to hover the aircraft at the same gross weight. If it is assumed that the resultant lift vectors for each blade are located at $0.75R$, then the change in propulsive force (reduction of drag) per blade in the x direction is given by

$$\Delta\bar{P}_x = \frac{\Delta\text{Torque}}{\text{q}(0.75R)} = 5.52 \text{ lb} \tag{20}$$

Nondimensionalizing the change in propulsive force per blade yields

$$\Delta C_{P_x} = \frac{\Delta\bar{P}_x}{\rho v^2 b} = \frac{\Delta\bar{P}_x}{\rho(0.75R\Omega)^2 b} = 0.037 \tag{21}$$

Thus, if unsteady aerodynamics can provide some insight into why the OH-6A had performance benefits, there must be a change in the propulsive force coefficient of the order of 10^{-2}. However, another question must be answered first: "From where does this propulsive force come?" Analysis of the data shows two possible sources: 1) increased blade motion (pitch and flapping) when HHC is turned on, and 2) wake phasing relationship based on the variation of input frequency to rotational frequency.

1. *Increased Blade Motion*

Figure 18 is a Southwell plot (or fan plot) for the OH-6A. It can be seen that both the 3P input frequency is very close to the second flapwise natural frequency at operational rpm, and the 5P input frequency is very close to the third flapwise natural frequency at operational rpm. It can be concluded that inputs at 3P and 5P would have greater flap deflections than inputs at other frequencies. In fact, the HHC flight-test data revealed an increase in the flap deflection for 1P, to 5P, harmonics when HHC was turned on with 1P being the predominant term. The flap deflection with HHC off was 3.1 in., and the flap deflection with HHC on was 4.0 in. at 0.75 chord, an increase of approximately 0.9 in. Nondimensionalizing by the semichord, the flap deflections would be 0.901 and 1.159 for HHC off and on, respectively.

Using the following parameters for the OH-6A in hover, a plot of the propulsive force coefficient against frequency ratio for HHC on is shown in Fig. 19: $h = 3.66$ (wake spacing), $k = 0.116$ (reduced frequency for 4P input), and $\alpha_0 = 0.33$ deg. This plot shows that given a 4P input, there exists a phase relationship that will yield a propulsive force of 10^{-2}, which could account for the performance improvement seen. Recall from Figs. 14 and 15 that plunge motion

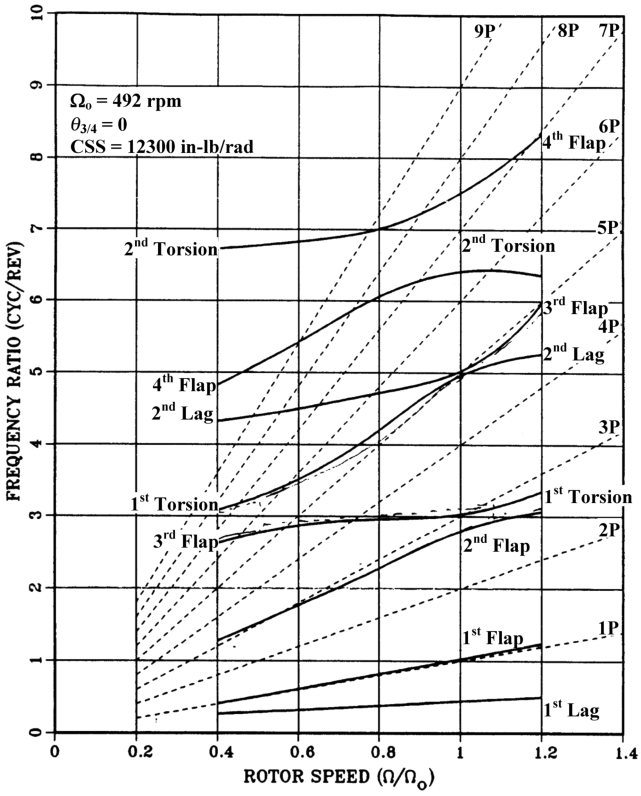

Fig. 18 Southwell plot for OH-6A.

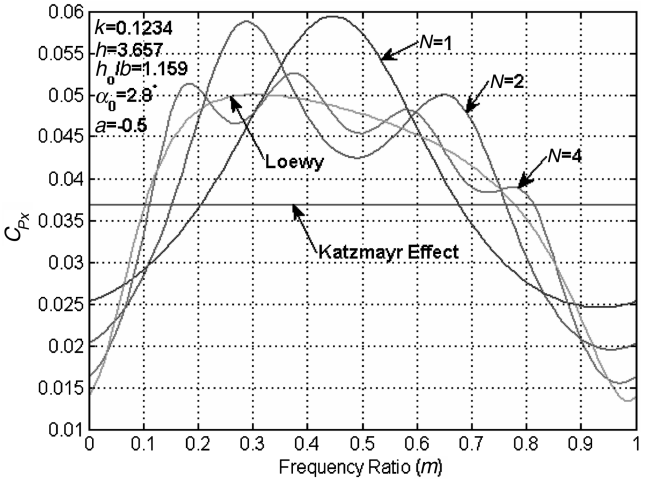

Fig. 19 Propulsive force coefficient for OH-6A with HHC on.

on the order of one semichord produces a much greater propulsive force than 1 deg of pitch motion and that coupled pitch–plunge motion is more than just the sum of individual pitch and plunge motions. Therefore, the increase in pitch motion must have provided a corresponding increase in blade flapping motion, and it is the coupling of these motions that provides a propulsive force of the order of magnitude seen with HHC turned on.

2. Wake Phase Relationship

Although increased blade motion alone could account for the increased performance, there might also be something in the manner by which the HHC inputs are made that provides insight into the variation seen, especially at the higher airspeeds. Recall from Fig. 4, it can be seen that not every controller phase relationship was equally effective in providing a performance benefit. Figure 19 shows that while coupled pitch–plunge oscillations had $C_{Px} \approx 10^{-2}$, the propulsive force coefficient varied from a high of 0.06 to a low of 0.013 as the frequency ratio varied. This would support the notion that although there is still a performance improvement with HHC on, the phasing relationship between the shed layers of vorticity plays an important role in determining how beneficial the performance improvement might be. Because of the limited performance test data from the HHC flight tests, it is difficult to ascertain what the exact benefits would be.

C. Other HHC Flight/Wind Tunnel Tests

Initial reports for the performance benefits seen on the OH-6A flight tests were met with some skepticism. Other helicopter manufacturers built their own versions of HHC, but they did not always achieve the same level of performance seen on the OH-6A. The Boeing Vertol Company built a scaled model of the three-bladed CH-47D with HHC installed [2]. To study performance aspects of HHC, a 2P [or $(q-1)$/rev] control input was applied at two cruise airspeeds. The power required at 135 knots was reduced by 6%, and the power required at 160 knots was reduced by 4%. However, control inputs of 2 deg were required to achieve the optimum reductions, and the frequency inputs required for the scaled model were much higher than the full-scale aircraft. Still the results appeared to substantiate the claims made on the OH-6A.

Flight tests on an SA-349 Gazelle by Aerospatiale [4] noted "only very low effects of higher harmonic control on piloting (pilot controls, aircraft attitude, and rotor power) could be observed". Flight tests on the S-76A by Sikorsky Aircraft [5,6] noted "no significant positive or negative effect on aircraft level flight performance."

The reason for this apparent disparity of results can be seen in the design and incorporation of the HHC actuators on these two aircraft compared to the OH-6A. The OH-6A HHC actuators shown in Fig. 1 were incorporated directly on the primary swashplate servos, ensuring that HHC inputs would be directly transmitted as blade angle motion. Additionally, as reported earlier, considerable effort was made to minimize the freeplay in the rotor and flight system to include replacing lightweight, but more flexible aluminum components with heavier, more rigid steel components. Both the SA-349 and S-76A mounted their actuators in series with the existing primary swashplate servos. This type of design inherently introduces one more component that could increase the freeplay of the rotor and flight control system. Because [4,6] do not mention any considerable effort to minimize freeplay, it may be assumed that it was not given the same level of attention that it was on the OH-6A. Additionally, the inputs used to achieve the same level of vibration reduction on the SA-349 and S-76A were greater than the OH-6A, lending more credence to the argument that freeplay was the reason the SA-349 and S-76A did not demonstrate the same performance benefits. In essence, any benefits that could have arisen as the result of optimally applying unsteady aerodynamics were absorbed by the freeplay in the flight control system.

V. Conclusions

Unsteady aerodynamics can play an important role in the application of HHC. The wake spacing, reduced frequency, and the phase angle relationship between input oscillations and rotational frequency have a significant effect on the rotary-wing lift deficiency functions. Changes in the lift deficiency function cause changes in the magnitude and phase relationships in the aerodynamic forces and moments that contribute to changes in the rotor system performance. The following conclusions can be drawn concerning unsteady aerodynamics as applied to HHC in hover:

1) For certain combinations of coupled pitch–plunge oscillations, rotary-wing unsteady aerodynamic theory predicts a propulsive force that reduces induced drag on the rotor.

2) If freeplay can by minimized, unsteady aerodynamic theory for a single wake predicts a propulsive benefit of the correct order of magnitude and phase relationship seen in the flight tests.

Further work concerning the performance benefits of HHC is warranted. The trends seen in hover could be extended to 60 and 80 knots using a modified version of the single-wake (or multiwake) theory that includes forward airspeed V and the nonperiodic nature of the blade motion ψ_q [14]. Recommendations are as follows:

1) Expand the finite-wake theory to calculate propulsive force (performance benefits) in forward flight and for rotor blades incorporating flaps for individual blade control (IBC).

2) Ensuring that freeplay is minimized, conduct flight tests to compare HHC optimized for performance improvements vs HHC optimized for vibration reduction to determine the correlation between performance and vibration reduction.

References

[1] Wood, E. R., Powers, R. W., Cline, J. H., and Hammond, C. E., "On Developing and Flight Testing a Higher Harmonic Control System," *Journal of the American Helicopter Society*, Vol. 30, No. 2, Jan. 1985, pp. 1–20.

[2] Cheng, R. P., Theodore, C. R., and Celi, R., "Effects of Higher Harmonic Control on Rotor Performance," *Proceedings of the 56th Annual Forum of the American Helicopter Society*, AHS International, Alexandria, VA, May 2000, pp. 18–27.

[3] Shaw, J., Albion, N., Hanker, E. J., and Teal, R. S., "Higher Harmonic Control: Wind Tunnel Demonstration of Fully Effective Vibratory Hub Force Suppression," *Journal of the American Helicopter Society*, Vol. 34, No. 1, 1989, pp. 14–25.

[4] Polychroniadis, M., and Achache, M., "Higher Harmonic Control: Flight Tests of an Experimental System on SA-349 Research Gazelle," *Proceedings of the 42nd Annual Forum of the American Helicopter Society*, AHS International, Alexandria, VA, June 1986.

[5] Miao, W., Kottapalli, S. B. R., and Frye, H. M., "Flight Demonstration of Higher Harmonic Control (HHC) on S-76," *Proceedings of the 42nd Annual Forum of the American Helicopter Society*, AHS International, Alexandria, VA, June 1986.

[6] Walsh, D. M., "Flight Tests of an Open Loop Higher Harmonic Control System on an S-76A Helicopter," *Proceedings of the 42nd Annual*

Forum of the American Helicopter Society, AHS International, Alexandria, VA, June 1986.

[7] Wood, E. R., Platzer, M. F., Abourahma, A., and Couch, M. A., "On the Unsteady Aerodynamics of Higher Harmonic Control," *Proceedings of the Nineteenth European Rotorcraft Forum*, No. C17, AHS International, Alexandria, VA, Sept. 1993, pp. C17-1–C17-25.

[8] Theodorsen, T., "General Theory of Aerodynamic Instability and the Mechanism of Flutter," NACA TR-496, 1935.

[9] Couch, M. A., "A Finite Wake Theory for Two-Dimensional Rotary Wing Unsteady Aerodynamics," M.S. Thesis, Naval Postgraduate School, Monterey, CA, Sept. 1993, pp. 10–42.

[10] Loewy, R. G., "A Two-Dimensional Approximation to the Unsteady Aerodynamics of Rotary Wings," *Journal of the Aeronautical Sciences*, Vol. 24, No. 2, Feb. 1957, pp. 81–92.

[11] Katzmayr, R., "Effect of Periodic Changes of Angles of Attack on Behavior of Airfoils," NACA TM-147, Oct. 1922.

[12] Garrick, I. E., "Propulsion of a Flapping and Oscillating Airfoil," NACA TR-567, 1936.

[13] Pang, K. C., "A Computer Code (USPOTF2) for Unsteady Incompressible Flow Past Two Airfoils," M.S. Thesis, Naval Postgraduate School, Monterey, CA, Sept. 1988.

[14] Shipman, K. W., and Wood, E. R., "A Two-Dimensional Theory for Rotor Blade Flutter in Forward Flight," *Journal of Aircraft*, Vol. 8, No. 12, Dec. 1971, pp. 1008–1015.